On the atomic structure of thiol-protected gold nanoparticles: a combined experimental and theoretical study†

M. M. Mariscal,*[ab] J. A. Olmos-Asar,[a] C. Gutierrez-Wing,[bc] A. Mayoral[b] and M. J. Yacaman[b]

Received 12th March 2010, Accepted 6th July 2010
DOI: 10.1039/c004229c

In the present work new findings on the structure of the S–Au interface are presented. Theoretical calculations using a new semiempirical potential, based on density functional theory and a bond-order Morse potential, are employed to simulate the adsorption process in a more realistic way. The simulation results reveal the formation of gold adatoms on the nanoparticle surface and high surface disorder due to the strong S–Au bond. Experimental data were acquired by aberration (Cs) corrected scanning transmission electron microscopy (STEM) using a high angle annular dark field detector (HAADF) that showed a great similarity with the theory predicted.

Introduction

Nanomaterials are of great interest in several research areas as well as in many technological applications, mainly due to their properties which specifically depend on their size and geometry. Those materials are useful when a high area/volume ratio is required. Some of their applications include biosensors, catalysis, drug "delivery" and construction of nano-circuits.[1–3]

Preparation, conservation and protection of metallic nanoparticles require passivation with organic ligand molecules if they will remain in a colloidal suspension. When nanoparticles are made of gold, a relatively easy way of protecting them is through organic molecular self-assembly, particularly with thiol molecules due to the strong interaction between sulfur and gold atoms. Self-assembly monolayers (SAMs) have been intensively studied, at experimental[4–6] and theoretical levels,[7–10] on extended gold (111) surfaces. Nevertheless, a clear understanding about some fundamental structural aspects of passivated Au nanoparticles in the range of 1–10 nm still does not exist.

From the theoretical side, the pioneer work was performed by Luedtke and Landman[11] where the structure, dynamics, and thermodynamics of gold nanocrystallites passivated by alkylthiolate monolayers were investigated by means of molecular dynamics simulations. In such studies gold atoms were kept constant during the whole dynamics simulation, and therefore no structural information about the gold nanoparticles was studied, necessary to understand the properties and structures of capped nanoparticles. Very recently, a great challenge in understanding the structure of the thiol/gold interface has been produced due to the experimental work of Kornberg and co-workers,[12] which has also induced a reconsideration of the planar Au(111)/thiol molecular junction.[13] Most of these experimental findings propose the existence of RS–Au_{adatom}–SR structural motifs on the gold surface, which represents a new picture of the Au/SR interface, which was recognized as thiol-terminal group bounded to fcc-bridge Au sites until 2007. The experiments performed by Kornberg and co-workers involve the crystallization and freezing of small Au_{102} clusters capped with *p*-mercaptobenzoic acid (*p*-MBA), an organic molecule which contains a benzene π-electron system and a carboxyl and thiol group. By means of X-ray crystal structure determination they were able to find, after 15 crystals screened, the atomic order in that explicit system, which *a priori* cannot be extended to larger nanoparticles. Several density functional calculations, starting with the crystalline structure found by Kornberg *et al.*, were rapidly performed in order to confront these experimental findings. Li *et al.*[14] have found excellent agreements with the experimental results confirming the stability of the crystallized structure. However, it must be noted that most of the theoretical predictions made for gold capped clusters ($n < 147$ atoms) were performed at the density functional level of theory, using optimization techniques unable to explore the complex energy landscape, and the obtained structures corresponded to local minima configurations at 0 K. Kinetic considerations are neglected in most of the theoretical works. More recently, careful studies from Murray's group[15] have experimentally confirmed the existence of semirings on $Au_{25}(SCH_2CH_2Ph)_{18}$ nanocrystals. In a parallel theoretical study, the energetic stability was established using DFT.[16]

Zachariah and coworkers[17] have also reported a semiempirical molecular dynamics study of an all-mobile-atom approach to study the mechano-chemical stability of thiol protected Au

[a] *INFIQC-CONICET, Departamento de Matemática y Física, Fac. Cs. Químicas, Universidad Nacional de Córdoba, (5000) Cordoba, Argentina. E-mail: marcelo.mariscal@gmail.com; Fax: +54 351-4344972; Tel: +54 351-4344972*
[b] *Department of Physics and Astronomy, University of Texas at San Antonio, One UTSA Circle, San Antonio, TX 78249, USA. E-mail: Miguel.Yacaman@utsa.edu*
[c] *Instituto Nacional de Investigaciones Nucleares Ciencias Aplicadas-Tecnología de Materiales, Carr. México-Toluca S/N, La Marquesa Ocoyoacac, Edo. de México 52750, Mexico*

† Electronic supplementary information (ESI) available: S1: particle size distribution, average size and standard deviation were based on the measurement of 303 nanoparticles. Random gold atom aggregates were not considered for statistics. S2: energy-dispersive X-ray (EDX) analysis of the thiol-capped Au nanoparticles. See DOI: 10.1039/c004229c

nanoparticles (NPs). In their work, they reported that the surface of gold nanoparticles becomes highly corrugated by the adsorption of thiol molecules. But, the interatomic potential chosen to describe the S–Au interface fails to represent the bond-order dependence of the S–Au bond, since they have used a classical Morse potential fitted to reproduce the adsorption energy of thiols on Au(111) perfect flat surfaces, and other local environment are not considered during the parameterization procedure. Despite the large amount of data available, the exact nature of the bonding between the molecules and the surface is not completely determined.

It is well known that the RS–Au bond in self-assembled monolayers has a large covalent character.[18] That means, that chemisorption exists, and that the bond is really complex for being correctly described. Theoretical calculations performed using *ab initio* methods show that the energy as well as the adsorption site of alkanethiols on metallic substrates depend on the coordination number of the thiolate groups as well of the Au atoms, *i.e.* to accurately describe the S–Au bond, the bond-order principle must be taken into account.[19,20] To the best of our knowledge, at present, two types of empirical interatomic potentials to describe the S–Au interface are found in the literature. These are mainly Morse-like potentials which have been fitted to reproduce alkanethiol adsorption on perfect, smooth, immobile Au(111) surfaces,[21] and low-dimensional systems.[22]

In the present work, we have tackled the study of the thiol/gold interface by realistic computer simulations and by advanced electron microscopy technique. We have used the two-phase method to produce thiol-capped Au nanoparticles with a narrow size distribution, which were subsequently characterized by electron microscopy, revealing a similarity between theory and experiments on distortion of the gold crystallites. Moreover, the high-resolution microscopy reveals the existence of small clusters and even isolated single gold atoms or Au(I)SR complexes.

We have also developed a new semi-empirical interatomic potential for the S–Au bond which is able to describe interacting species with bond order dependence. The new potential is used in combination with force-fields and the second-moment approximation of the tight binding to reproduce the adsorption of *n*-alkanethiol molecules on Au NPs by means of Langevin dynamics simulations (LD).

Methods

Experimental

Gold nanoparticles passivated by 1-dodecanethiol were synthesized by a phase transfer procedure following the Brust method[23,24] and increasing the S : Au molar ratio used.[25,26] The reaction proceeded at room temperature under vigorous stirring by adding 2 ml of a 0.1 M aqueous solution of hydrogen tetrachloroaurate trihydrate ($HAuCl_4{\cdot}3H_2O$) to 20 ml of toluene containing 1.0 mmol of dissolved tetraoctylammonium bromide ($N[C_8H_{17}]_4Br$). Then, 0.3 ml of 1-dodecanethiol ($C_{12}H_{25}SH$) and 6 ml of a 0.4 M aqueous solution of sodium borohydride ($NaBH_4$) were added. The reaction proceeded for 3 h. The passivated nanoparticles were purified by precipitation in ethanol from the organic phase and redispersed in toluene. All chemicals were purchased from Aldrich and used without any further purification. 5 mg of the resulting passivated nanoparticles were suspended in 15 ml of toluene containing 86 mg of graphite and heated at 50 °C for 3 h. A drop of this suspension was deposited over a TEM carbon coated copper grid and the solvent was allowed to dry.

Samples were analyzed by scanning transmission electron microscopy in a JEOL 2200FS Scanning Transmission Electron Microscope (STEM) with a hexapole corrector (CEOS GmbH) for the electron probe. The geometric aberrations of the probe-forming system were controlled to allow a beam convergence of 26.5 mrad half-angle to be selected. The high angle annular dark field (HAADF) images were acquired from 100 to 170 mrad scattering semi-angle, easily satisfying the requirement for the detector to eliminate contributions from unscattered or low-angle scattered.

The alignment of the microscope was verified through the CESCOR software. A focus/tilt tableau was acquired measuring defocus and two-fold astigmatism as a function of both radial and azimuthal tilt. In order to 'clean' the raw data and to reduce the noise of the images recorded, the images were filtered using the Richardson–Lucy algorithm implemented by Ichizuka.[27]

Simulation method

As mentioned above, aside density functional calculations, most of the computer simulations performed to study the adsorption of alkanethiols on gold surfaces have been tackled using the simple pairwise Morse potential. Nevertheless, this potential cannot describe in a correct way the adsorption behavior of these molecules on other systems, like (100) crystalline surfaces or surface defects, and especially those of low dimensionality, such as gold nanowires or nanoparticles. For example, it was recently found that adsorption of thiolates on gold adatoms is energetically more stable than adsorption on flat surfaces.[28] Moreover, the simple pairwise Morse potential predicts a low adsorption energy on this site (on-top a Au adatom); due to the fact that the bond-order of sulfur is equal to one, as in an on-top perfect surface site.

Our goal was to introduce a bond-order n_j dependence on D_e and r_e parameters of the Morse function. The first one takes into account the binding energy and the second one the equilibrium S–Au bond distance. The potential is described by the following functional form:

$$V_{S\text{–}Au} = D_e(n_j)\exp[-\alpha(r - r_e(n_j))]\{\exp[-\alpha(r - r_e(n_j))] - 2\} \quad (1)$$

where D_e, α, and r_e are fitted parameters and the bond-order is calculated as follow:

$$n_j = \sum_{i \neq j} f(r_{ij}) \quad (2)$$

$$f(r) = \left\{ \begin{array}{l} 1 \\ 0 \\ \frac{1}{2} - \frac{1}{2}\sin\left[\frac{\pi(r - R_{mid})}{C_2 - C_1}\right] \end{array} \right\} \begin{array}{c} r \leq C_1 \\ r \geq C_2 \\ C_1 < r < C_2 \end{array}$$

where we have taken $C_1 = 2.900$ Å and $C_2 = 3.187$ Å.

This journal is © the Owner Societies 2010

Six adsorption sites on different substrates were considered during the fitting procedure: two mono-coordinated sites—*on-top* in a perfect (111) flat surface and on an adatom; one bi-coordinated site—*bridge* position on a perfect (111) surface-; one tri-coordinated site—*hollow* position in a (111) surface-; a tetra-coordinated site—*hollow* position in a perfect (100) surface and the staple motifs (RS–Au–SR). In each selected configuration, with the molecule/s adsorbed on the equilibrium position (it implies S–Au distance at the r_e value), the parameter D_e was changed self-consistently, keeping α as a constant, until our results reproduce the value of the adsorption energy predicted by ab-initio calculations.[19,29] As mentioned above we have introduced the novel structural motif (RS–Au–SR) in our parameterization procedure in order to reproduce its energetic stability. In a first test, simulated annealing was performed for one methanethiolate molecule adsorbed between two Au adatoms on a Au(111) surface as shown in Fig. 1.

The calculated adsorption energy with our potential is −2.728 eV per RS, in very good agreement with the value reported by Jiang *et al.*[30] of −2.77 eV per RS for a similar structure. In a second test, the "staple" motif, RS–Au–SR (see Fig. 2), was used to calculate the adsorption energy per SCH_3 species.

The adsorption energy calculated with our potential is −2.217 eV per RS, in good agreement with the DFT value reported by Jiang[30] of −2.22 eV per RS and considerably more favorable than the "standard" fcc-bridge site (−1.84 eV per SR). We have found that both CH_3S– groups are attached to the terrace gold atoms with a Au–S bond length of 2.55 Å, and to the Au adatom with a Au–S bond length of 2.35 Å, in very good agreement with DFT results.

Having these parameters, cubic spline interpolations are performed to obtain values at intermediate positions while satisfying the continuity of the potential energy landscape. To assure continuity of the potential in the cutoff, the modified Morse function is splined at long distances.

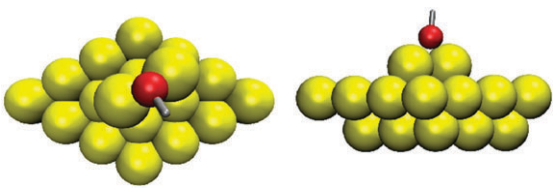

Fig. 1 Geometric configuration of the Au–SR–Au structural motif on Au(111) surfaces. Left: top-view, right: lateral view. (Yellow spheres: Au atoms, red: S and silver bar: alkane-chain.)

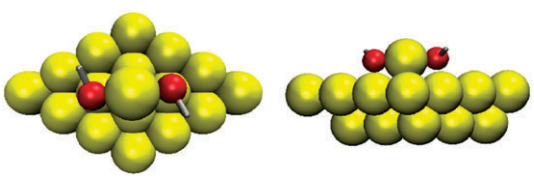

Fig. 2 Geometric configuration of the RS–Au–SR staple motif on Au(111) surfaces. Left: top-view, right: lateral view. (Yellow spheres: Au atoms, red: S and silver bars: alkane-chain.)

The Au–Au interactions were modeled using the second-moment approximation of the tight binding theory[31] which takes into account the many-body character of the metallic bond. The intra and intermolecular interactions of the thiol molecules were represented by means of the Universal Force Field (UFF)[32] which has been shown to reproduce the main properties of the alkyl chain. The parameters to represent the intermolecular interactions have been taken from Hautman and Klein[7] which represent correctly the chain–chain interaction and the orientation of the molecules with respect to the gold surface.

The solvent is represented indirectly as a thermal bath which induces stochastic motion in these regions. Thus, the particles obey Langevin dynamics according to:

$$\frac{dv_i}{dt} = -\xi v_i + F_S + F_R \qquad (3)$$

where v_i is the velocity of particle i, ξ is the friction coefficient, F_R represents the random force acting on each particle and F_S the systematic force described by the summation of the semiempirical potentials described above. The friction constant ξ and the random force F_R are related by the fluctuation–dissipation theorem. The Brownian dynamics were implemented by Ermak's algorithm.[33]

Result and discussions

Experimental

Gold nanoparticles passivated by 1-dodecanethiol were obtained with a narrow size distribution of the crude product (Fig. 3a). An average size of 2.3 nm with a standard deviation of 0.49 was determined (see ESI† S1). Detailed HRTEM analysis shows that the structures of these nanoparticles include FCC (cubo-octahedra, truncated octahedra), decahedra and some icosahedra (Fig. 3b and c), where the surface of the particles contains adatoms that do not retain the same interatomic distance reported for gold, as observed by HAADF. These adatoms were found in planes (111) and (100) which correspond to the exposed planes of the identified nanostructures.

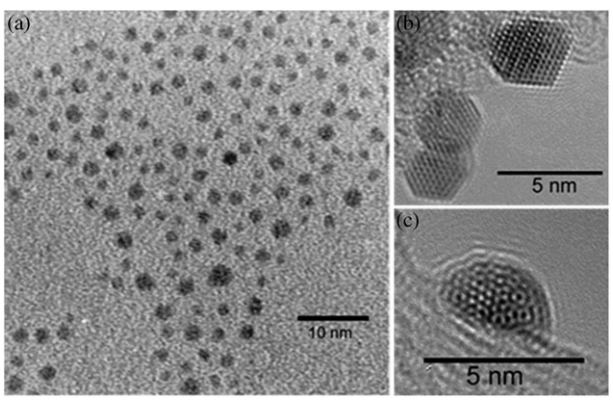

Fig. 3 Gold nanoparticles capped with 1-dodecanethiol. (a) General view; (b and c) HRTEM images of nanoparticles with a FCC and icosahedral structures respectively.

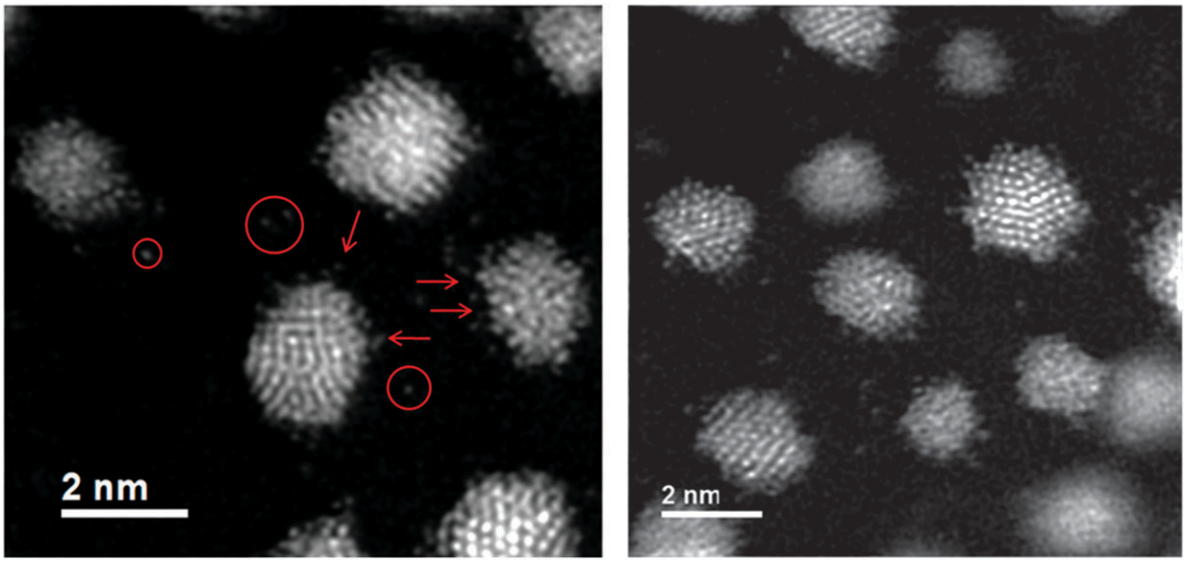

Fig. 4 Aberration corrected high resolution STEM-HAADF images of 1-dodecanethiol capped Au nanoparticles. The circles indicate the possibility of small nucleus of 2–3 atoms and the red arrows remark the formation of defect in the surface of the nanoparticles, like gold adatoms.

However, not all the observed particles have well defined shapes. A fraction of nanoparticles smaller than 2 nm was identified, where some showed large distortions that did not allow associating them to a specific crystalline structure. Also, it is observed that few atoms tend to aggregate into clusters or amorphous structures of less than 1 nm, along with some other isolated gold atoms (see Fig. 4).

Electron microscope images were recorded in STEM mode, simultaneously, in both bright field and dark field modes. With the high angle annular dark field detector the electrons that have undergone high angle scattering and are highly incoherent are used to create the images. In this mode heavy elements such as metals appear much brighter with respect to light elements such as carbon.

Fig. 4 depicts the high resolution Cs corrected STEM-HAADF images of gold nanoparticles of a maximum size of 2 nm. Isolated atoms or maybe Au(SR) complexes are also formed (marked by circles). The disrupted surfaces created on the gold nanocrystals are marked by arrows. The images were commonly recorded for 15 to 20 s with no apparent change on the structure suggesting that the surface disorder (*i.e.* heterogeneities on the atomic scale) could be owed to the S atoms linked to the Au. Energy-Dispersive X-ray (EDX) analysis have been performed during SEM measurements under STEM dark field mode. As can be observed in Fig. S2 (ESI†) a considerable amount of sulfur has been detected with a 60–40 atomic composition with respect to gold.

Theoretical results

In order to study the effect of thiol molecules when protecting the gold nanoparticles, we have performed a series of Langevin dynamics simulations to obtain the dynamic evolution of the adsorption process at constant temperature (300 K). The simulations were conducted as follows:

(a) First, we performed quenching molecular dynamics and energy minimizations using the LBFGS quasi-Newtonian nonlinear optimization algorithm[34] to find the relaxed structures of the gold bare nanoparticles.

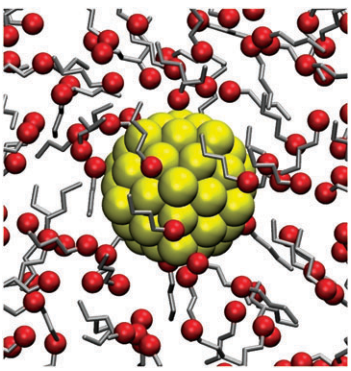

Fig. 5 Typical initial configuration of a gold nanoparticle surrounded by *n*-butanethiolate molecules before running a Langevin dynamics simulation. (Yellow spheres: Au atoms, red: S and silver bars: alkane-chain.)

(b) Secondly, an excess of randomly distributed butanethiolate molecules $[CH_3(CH_2)_3S]$ are created around the relaxed Au NP (see Fig. 5). Within this approach, the adsorption sites are not assumed *a priori*. Moreover, concerted diffusion processes are allowed during the dynamics evolution, a key way, absent in most of the deterministic methods, involving ''one-to-one'' movements during the optimization procedure.

(c) Finally, a Langevin dynamics simulation is performed during 1 ns in order to mimic the adsorption of the *n*-butanethiolate molecules including the effect of the solvent molecules through stochastic and frictional forces.

(d) As stated above, Langevin dynamics simulations have been performed for several gold nanoparticles of the first members of the icosahedra family, *i.e.* Au_{13}, Au_{55}, Au_{147}, Au_{309}, Au_{561}, Au_{923} and Au_{1415}, which correspond to a range of diameters between 1–4 nm. Fig. 6 shows some selected snapshots of the initial and final configuration of the simulation

 This journal is © the Owner Societies 2010

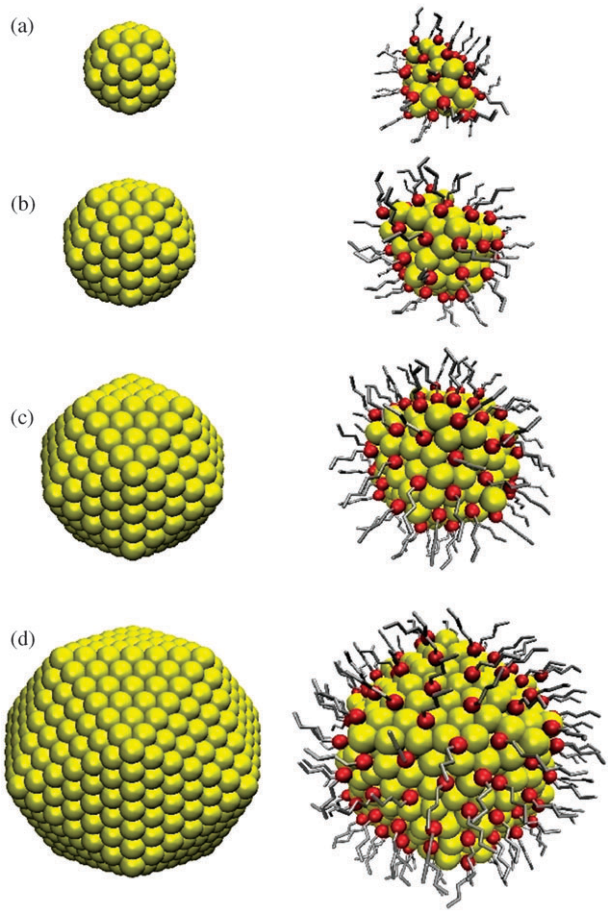

Fig. 6 Initial (left) and last (right) configurations taken from the Langevin dynamics simulation after adsorption of butanethiolate molecules. (a) Au_{55}–$(SR)_n$, (b) Au_{147}–$(SR)_n$, (c) Au_{309}–$(SR)_n$, (d) Au_{923}–$(SR)_n$ at 300 K. See the text for details. (Yellow spheres: Au atoms, red: S and silver bars: alkane-chain.)

after 1 ns. As can be seen on the figure, as the nanoparticle diameter decreases, a very strong surface disorder is observed, a phenomenon that fairly disappears as the particle size increases.

For instance, in the case of Au_{55}, the icosahedra structure is completely lost due to the strong S–Au interaction, comparable in magnitude to the Au–Au interaction on the outer layers of the gold nanoparticles (see Table 1).

At 300 K, there is a competition between perpendicular bonding (S–Au) and lateral ones (Au–Au). In Fig. 6, the atomic structure of Au_{147}–$(SR)_n$ and Au_{309}–$(SR)_n$, frames (b) and (c), also reveals the formation of gold adatoms (characterized

Table 1 Internal energy of gold atoms on different sites according to the Second Moment Tight Binding potential (SMTB) and binding energy of S–Au on flat (111) surface and on-top Au adatoms according to our potential

Site	Energy/eV
Au on Au(111) facets	−3.44
Au on borders	−3.12
S–Au(111)	−1.84
S–Au(adatom)	−2.93

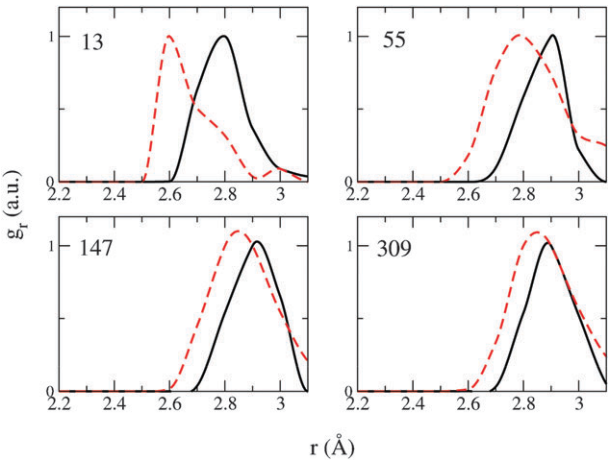

Fig. 7 Nearest neighbor's distribution for 1-butanethiol capped gold nanoparticles (dashed red lines) and bare gold NPs (full black line) for different core sizes (Au_{13}, Au_{55}, Au_{147}, Au_{309}). Langevin dynamics conditions: 300 K and $\xi = 100\ ps^{-1}$.

by the low coordination number), which in most cases are bonded to one or two thiolate molecules. Several RS–Au–SR structural motifs are formed during the LD simulation. However, due to the fact that thermal effects are present in our simulation model, a well-defined structure cannot be captured. In the case of Au_{923}–$(SR)_n$ the surface of the particle appears slightly disordered, but the internal core keeps the icosahedra structure. A remarkable feature of all of these simulations is the self-assembly of the alkane chains due to the collective van der Waals interactions.

It is interesting to point out the agreement of our results to those reported by Garzón *et al.*,[35] where by means of DFT calculations, they have found that the effect of a methylthiol monolayer, approximately 24 SCH_3 molecules on a Au_{38} cluster, is strong enough to produce a dramatic distortion on the gold cluster, resulting in a disordered geometry for the most stable $Au_{38}(SCH_3)_{24}$ capped nanoparticle.

Closer inspection of the atomic configurations, by means of computing the pair distribution function, reveals a contraction of the Au–Au distance, with respect to the equilibrium Au–Au distance in bare clusters, as the particle size decreases. Fig. 7 shows the first nearest neighbor's distribution of Au–Au bonds for the first four members of the icosahedra family.

As can be observed in Fig. 7, the maximum of the peak is displaced to lower values as the nanoparticle diameter decreases. It is interesting to note that when the diameter of the nanoparticles is around 2.2 nm (~309 atoms) the Au–Au contraction is released, due to the many-body character of the metallic bond.

Conclusions

In the present study we have shown theoretical evidence confirming the strong surface disorder on the structure of thiol protected gold nanoparticles in the range 1–4 nm. The high resolution electron microscopy images obtained were in agreement with the theory proposed revealing that when the nanoparticles size is lower than 2–3 nm the surface of the

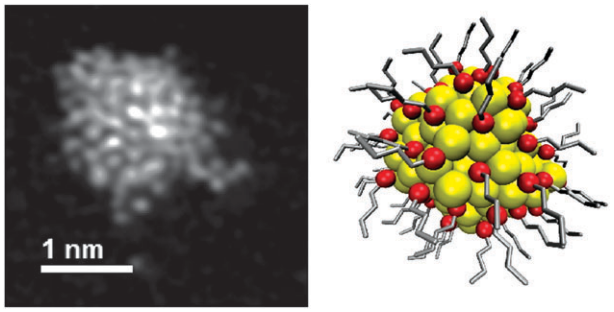

Fig. 8 A comparison between an experimental and a theoretical structure of a gold nanoparticle capped by alkanethiol molecules of similar size.

nanoparticles was highly disordered. In addition, when the gold clusters were smaller than 2 nm, a crystalline structure could not be resolved. Evidence of small Au nucleus and isolated adatoms and chain of gold with unusual Au–Au distances were also observed.

Langevin dynamics simulations using a new semi-empirical approach to realistically describe the complex S–Au energy landscape are used to explore the structure of butanethiolate capped Au nanoparticles, in the range 1–4 nm. In general terms, a very good agreement has been found between the structures of the synthesized nanoparticles and that simulated. For a direct comparison, in Fig. 8, two Au nanoparticles of similar size are shown. As can be seen the structure of the particles presents the same structural behavior, *i.e.* a strong surface disorder with the formation of Au ad atoms.

Acknowledgements

M.M.M. wishes to thank CONICET, Welch foundation agency project #AX-1615, to the ICNAM of the University of Texas, Secyt-UNC, Program BID (PICT 2007-00340, 2006-0946 and PME 2006-1581) for financial support. J.A.O.-A. thanks CONICET for the fellowship. The authors would also like to thank Dr Larry F. Allard for technical support.

Notes and references

1 A. Manna, T. Imae, K. Aoi and M. Okazaki, *Mol. Simul.*, 2003, **29**, 661–665.
2 R. Hong, G. Han, J. M. Fernández, B. Kim, N. S. Forbes and V. M. Rotello, *J. Am. Chem. Soc.*, 2006, **128**, 1078–1079.
3 M. M. Mariscal and S. A. Dassie, *Recent Advances in Nanoscience*, Research Signpost Pub., Trivandrum, India, 2007.
4 A. Ulman, S. D. Evans, Y. Shnidman, R. Sharma, E. Eilers and J. C. Chang, *J. Am. Chem. Soc.*, 1991, **113**, 1499–1506.
5 D. J. Lavrich, S. M. Wetterer, S. L. Bernasek and G. Scoles, *J. Phys. Chem. B*, 1998, **102**, 3456–3465.
6 C. Vericat, G. A. Benitez, D. E. Grumelli, M. E. Vela and R. C. Salvarezza, *J. Phys.: Condens. Matter*, 2008, **20**, 184004.
7 J. Hautman and M. Klein, *J. Chem. Phys.*, 1989, **91**, 4994–5001.
8 A. Pertsin and M. Grunze, *Langmuir*, 1994, **10**, 3668–3674.
9 Y. Yourdshahyan and A. M. Rappe, *J. Chem. Phys.*, 2002, **117**, 825–833.
10 M. J. Esplandiu, M. L. Carot, F. P. Cometto, V. A. Macagno and E. M. Patrito, *Surf. Sci.*, 2006, **600**, 155–172.
11 W. D. Luedtke and U. Landman, *J. Phys. Chem.*, 1996, **100**, 13323–13329.
12 P. D. Jadzinsky, G. Calero, C. J. Ackerson, D. A. Bushnell and R. D. Kornberg, *Science*, 2007, **318**, 430–433.
13 A. Cossaro, R. Mazzarello, R. Rousseau, L. Casalis, A. Verdini, A. Kohlmeyr, L. Floreano, S. Scandolo, A. Morgante, M. L. Klein and G. Scoles, *Science*, 2008, **321**, 943–946.
14 Y. Li, G. Galli and F. Gygi, *ACS Nano*, 2008, **2**, 1896–1902.
15 M. W. Heaven, A. Dass, P. S. White, K. M. Holt and R. W. Murray, *J. Am. Chem. Soc.*, 2008, **130**, 3754–3755.
16 J. Akola, M. Walter, R. L. Whetten, H. Hakkinen and H. Gronbeck, *J. Am. Chem. Soc.*, 2008, **130**, 3756–3757.
17 B. J. Henz, T. Hawa and M. R. Zachariah, *Langmuir*, 2008, **24**, 773–783.
18 N. Gonzalez-Lakunza, N. Lorente and A. Arnau, *J. Phys. Chem. C*, 2007, **111**, 12383–12390.
19 F. P. Cometto, P. Paredes Olivera, V. A. Macagno and E. M. Patrito, *J. Phys. Chem. B*, 2005, **109**, 21737–21748.
20 A. Bencini, G. Rajaraman, F. Totti and M. Tusa, *Superlattices Microstruct.*, 2009, **46**, 4–9.
21 R. Mahaffy, R. Bhatia and B. J. Garrison, *J. Phys. Chem.*, 1997, **101**, 771–773.
22 K. S. S. Liu, C. W. Yong, B. J. Garrison and J. C. Vickerman, *J. Phys. Chem. B*, 1999, **103**, 3195–3205.
23 M. Brust, M. Walker, D. Bethell, D. J. Schiffrin and R. Whyman, *J. Chem. Soc., Chem. Commun.*, 1994, 801.
24 C. Gutiérrez-Wing, P. Santiago, J. A. Ascencio, A. Camacho and M. J. Yacamán, *Appl. Phys. A: Solid Surf.*, 2000, **71**, 237–243.
25 T. G. Schaaff, M. N. Schafigullin, J. T. Khoury, I. Vezmar, R. L. Whetten, W. G. Cullen, P. N. First, C. Gutierrez-Wing, J. Ascencio and M. J. Jose-Yacaman, *J. Phys. Chem. B*, 1997, **101**, 7885–7891.
26 R. L. Whetten, J. T. Khoury, M. M. Alvarez, S. Murthy, I. Vezmar, Z. L. Wang, P. W. Stephens, C. L. Cleveland, W. D. Luedtke and U. Landman, *Adv. Mater.*, 1996, **8**, 428.
27 www.hremresearch.com.
28 P. Maksymovych, D. C. Sorescu and J. T. Yates, *Phys. Rev. Lett.*, 2006, **97**, 146103.
29 The adsorption energy of RS/Au(100) and the staple motif (RS–Au–SR)/Au(111) was calculated by us, using DFT/GGA within the effective core potential approach and double ζ-polarization basis set.
30 D.-e. Jiang, M. L. Tiago, W. D. Luo and S. Dai, *J. Am. Chem. Soc.*, 2008, **130**, 2777–2779.
31 F. Cleri and V. Rosato, *Phys. Rev. B: Condens. Matter*, 1993, **48**, 22–33.
32 A. K. Rappe, C. J. Casewit, K. S. Colwell, W. A. Goddard III and W. M. Skiff, *J. Am. Chem. Soc.*, 1992, **114**, 10024–10035.
33 M. P. Allen and D. J. Tildesley, *Computer Simulation of Liquids*, Clarendon Press, Oxford, 1987.
34 J. Nocendal and S. J. Wright, *Numerical Optimization*, Springer, New York, 1999, p. 224.
35 I. L. Garzón, J. A. Reyes-Nava, J. I. Rodríguez-Hernández, I. Sigal, M. R. Beltrán and K. Michaelian, *Phys. Rev. B: Condens. Matter Mater. Phys.*, 2002, **66**, 073403.

 This journal is © the Owner Societies 2010